NATIONAL ADVISORY COMMITTEE FOR AERONAUTICS

TECHNICAL NOTE 3753

AERODYNAMIC CHARACTERISTICS AND FLYING QUALITIES OF A

TAILLESS TRIANGULAR-WING AIRPLANE CONFIGURATION AS

OBTAINED FROM FLIGHTS OF ROCKET-PROPELLED MODELS

AT TRANSONIC AND LOW SUPERSONIC SPEEDS

By Grady L. Mitcham, Joseph E. Stevens,
and Harry P. Norris

Langley Aeronautical Laboratory
Langley Field, Va.

NACA

Washington

November 1956

NATIONAL ADVISORY COMMITTEE FOR AERONAUTICS

TECHNICAL NOTE 3753

AERODYNAMIC CHARACTERISTICS AND FLYING QUALITIES OF A

TAILLESS TRIANGULAR-WING AIRPLANE CONFIGURATION AS

OBTAINED FROM FLIGHTS OF ROCKET-PROPELLED MODELS

AT TRANSONIC AND LOW SUPERSONIC SPEEDS[1]

By Grady L. Mitcham, Joseph E. Stevens,
and Harry P. Norris

SUMMARY

A flight investigation has been made at the Langley Pilotless Air-
craft Research Station at Wallops Island, Va., to determine the aero-
dynamic characteristics of models of a tailless triangular-wing airplane
configuration. The results from three successful flight tests are pre-
sented for the Mach number range between 0.75 and 1.28.

The data showed that the models tended to tuck under slightly
through the transonic region. The variation of lift coefficient with
angle of attack was linear within the range of angles tested and the
lift-curve slope increased gradually between Mach numbers of 0.88
and 1.00.

The hinge-moment coefficients increased rapidly between Mach num-
bers 0.85 and 1.15 but showed a gradual decrease above a Mach number
of 1.20. Elevator effectiveness decreased approximately 40 percent
through the transonic region.

The models exhibited static and dynamic longitudinal stability
throughout the test Mach number range with the center of gravity located
at 20 and 25 percent mean aerodynamic chord. The aerodynamic center
showed a gradual rearward movement of about 15 percent mean aerodynamic
chord in the transonic region. All the models possessed directional
stability throughout the angle-of-attack and speed ranges of the flight
tests.

An analysis of the flying qualities of a full-scale configuration has been made from the data obtained from the three flight-test models. The analysis indicates adequate elevator control for trim in level flight over the speed range investigated. Through the transonic range there is a mild trim change with a slight tucking-under tendency. The elevator-control effectiveness in the supersonic range is reduced to about one-half the subsonic value, although sufficient control for maneuvering is available as indicated by the fact that 10° elevator deflection would produce 5g normal acceleration at a Mach number of 1.2 at an altitude of 40,000 feet. The elevator control forces are high and indicate the need of a control-boost system as well as the power required of such a system. The damping of the short-period oscillation is adequate at sea level and at 40,000 feet.

INTRODUCTION

The National Advisory Committee for Aeronautics is conducting a flight investigation of rocket-propelled models of a tailless triangular-wing airplane configuration to evaluate stability and control at low supersonic and transonic speeds. Results obtained from the successful flight tests of three models served as a basis for the analyses presented in this paper.

For the flight tests of the models, the program for control movement included abrupt pull-ups and push-downs with the elevons operated as elevators. The present paper contains the results of an analysis of the aerodynamic characteristics and the stability derivatives evaluated from the flight tests of the three rocket-propelled models and an analysis of the flying qualities of such an airplane in the Mach number range from 0.75 to 1.2. The flying qualities are based on an assumed triangular-wing airplane with a wing loading of 27.3 pounds per square foot at sea level and at a 40,000-foot altitude. The computations are based on two center-of-gravity positions, 20 and 25 percent of the mean aerodynamic chord.

SYMBOLS

A   amplitude of a short-period oscillation

a   velocity of sound, ft/sec

a_l longitudinal accelerometer reading, ft/sec^2

a_n normal accelerometer reading, ft/sec^2

a_t transverse accelerometer reading, ft/sec^2

$C_{1/2}$ cycles for short-period oscillation to damp to one-half amplitude

C_c chord-force coefficient, positive in a forward direction, $\dfrac{a_l}{g} \dfrac{W}{S} \dfrac{1}{q}$

C_h total hinge-moment coefficient

C_{h_α} rate of change of hinge-moment coefficient with angle of attack, per degree

C_{h_δ} rate of change of hinge-moment coefficient with elevator deflection, per degree

C_{h_0} basic hinge-moment coefficient at zero angle of attack and zero elevator deflection

C_L lift coefficient, $C_N \cos \alpha + C_c \sin \alpha$

C_{L_α} rate of change of lift coefficient with angle of attack, per degree

C_{L_δ} rate of change of lift coefficient with elevator deflection for a constant angle of attack, per degree

$C_{L_{trim}}$ trim lift coefficient

$C_{L_{\delta_{trim}}}$ rate of change of total lift coefficient between two trim conditions or elevator deflections, per degree

C_m pitching-moment coefficient

C_{m_0} basic untrimmed pitching-moment coefficient at zero angle of attack and zero elevator deflection

$\left(C_{m_\delta}\right)_{\alpha=K}$ rate of change of pitching-moment coefficient with elevator deflection for constant angle of attack, per degree

C_{m_α} rate of change of pitching-moment coefficient with angle of attack, per degree

$C_{m_{\dot{\alpha}\bar{c}/2V}} = \dfrac{\partial C_m}{\partial(\dot{\alpha}\bar{c}/2V)}$, per radian

C_{m_θ} rate of change of pitching-moment coefficient with pitch angle

$C_{m_{\dot{\theta}\bar{c}/2V}} = \dfrac{\partial C_m}{\partial(\dot{\theta}\bar{c}/2V)}$, per radian

C_N normal-force coefficient, $\dfrac{a_n}{g}\dfrac{W}{S}\dfrac{1}{q}$

$\bar{c}$ mean aerodynamic chord, 2.19 ft

d distance between center of pressure of angle-of-attack vane and center of gravity of model, ft

$\dfrac{d\delta}{d\alpha}$ rate of change of elevator deflection with angle of attack (due to flexibility of control system)

$\dfrac{dC_m}{dC_L}$ rate of change of pitching-moment coefficient with lift coefficient

F stick force, lb

g acceleration due to gravity, 32.2 ft/sec^2

H hinge moment, in-lb; total impact pressure (eqs. (1) and (2)), lb/sq ft

I_Y moment of inertia about pitch axis, slug-ft^2

K constant

M Mach number

m mass of model, lb-sec^2/ft

P period of an oscillation, sec

p free-stream static pressure, lb/sq ft

q dynamic pressure, $\dfrac{\gamma p M^2}{2}$, lb/sq ft

R   Reynolds number, $\dfrac{\rho V \bar{c}}{\mu}$

S   wing area, 6.25 sq ft

$T_{1/2}$ time to damp to one-half amplitude, sec

t   time from launching, sec

V   velocity, ft/sec

W   weight of model, lb

x   stick movement, in.

α angle of attack corrected for flight-path curvature and
            angular velocity, deg

α_i angle of attack as measured during flight, deg

α_{trim} trim angle of attack, deg

$\dfrac{\dot{\alpha}\bar{c}}{2V}$ nondimensional rate of change of angle of attack

$\left(\dfrac{\Delta\alpha}{\Delta\delta}\right)_{trim}$ rate of change of angle of attack with elevator deflection
            between two trim conditions

δ control deflection measured on chord line parallel to the
            plane of symmetry (positive with trailing edge down), deg

δ_{trim} trim elevator deflection, deg

γ specific-heat ratio (value taken as 1.40)

θ pitch angle, deg

$\dfrac{\dot{\theta}\bar{c}}{2V}$ nondimensional angular velocity of pitch

μ viscosity, slug/ft-sec

ρ mass density of air, slugs/cu ft

Subscripts:

1,2   conditions brought about by change in elevator deflection (see
              fig. 39)

a   full-scale airplane

m   model

Dots over a quantity represent derivatives of the quantity with
respect to time.

MODELS AND APPARATUS

The models had a wing of triangular plan form with 60° sweepback of
the leading edge and an aspect ratio of 2.31, the profile at all spanwise
stations being an NACA $65_{(06)}$-006.5 section. Longitudinal control was
provided by a single set of constant-chord trailing-edge control surfaces
on the wing called elevons. Deflecting the elevons together provides
longitudinal control and, in the assumed airplane, deflecting them dif-
ferentially would give lateral control. The vertical fin of the models
was of triangular plan form with a leading-edge sweepback of 60°.

A three-view drawing of the models used in the present investigation
is given in figure 1 and the physical characteristics of the models and
a full-scale representative tailless triangular-wing airplane are pre-
sented in table I. Photographs of one of the models are shown in figures 2
and 3. The model fuselage and components were constructed of duralumin,
magnesium castings, and magnesium skin. The fuselage construction was of
the monocoque type divided into three sections. The three sections were
the nose section which held the telemeters, the center section which held
the wings, vertical fin, compressed-air supply, and control-actuating
system, and the tail section which contained the rocket motor and booster
attachment.

The planned movement of the elevons called for abrupt pull-ups and
push-downs operating at a frequency of about 1 cycle in 1.2 seconds and
was accomplished by a compressed-air system. The control surfaces, which
were unsealed, moved together between stops in an approximately square-
wave motion. On model 1 the surfaces were deflected down 5.3° and up 5.3°;
on model 2 the deflection was down 4.7° and up 4.7°; and on model 3 the
deflection was down 1.1° and up 5.2°. The controls were in operation
during the entire flight.

The models were boosted to supersonic speeds by a solid-fuel, 6-inch-
diameter Deacon rocket motor which is capable of producing an average

thrust of 6,500 pounds for approximately 3.1 seconds. The rocket-sustainer motor for the model was a 5-inch solid-fuel high-velocity aircraft rocket shortened to 17 inches and modified to give an average thrust of 900 pounds for 1.4 seconds. The small sustainer motor served a two-fold purpose: (1) during the power-on portion of the flight it prevented immediate deceleration after separation and allowed the controls to operate one complete cycle at approximately a constant Mach number, and (2) it assured a positive separation between model and booster at booster burnout. The sustainer-motor nozzle served as the point of attachment of the booster to the model. This type of attachment also allowed a separation of the booster from the model if the ratio of drag to weight of the model and booster were favorable.

The booster-model combination was ground launched from a crutch-type launcher, as shown in figure 4. The launching angle from the horizontal for model 1 was $43^\circ 40'$, for model 2 was $44^\circ 40'$, and for model 3 was $43^\circ 23'$. Table II presents the weight and balance data for the models and the full-scale airplane. Figure 5 shows a sequence of photographs of one booster-model combination at take-off.

The data from the flights were obtained by the use of telemeters, CW Doppler velocimeter radar, photography, and radiosondes. The time histories of the data as the models traversed the Mach number range were transmitted and recorded by a telemeter system which gave eight channels of information. The data recorded were longitudinal, transverse, and normal acceleration; hinge moment; control position; angle of attack; total pressure; and a reference static pressure used to determine free-stream static pressure. Figure 6 shows the instrumentation arrangement on a typical model. Angles of attack were obtained by a vane-type angle-of-attack indicator located on a sting ahead of the nose of the model. A description of this indicator can be found in reference 1. The angle-of-attack range covered by the indicator with the vane located on the center line of the model was approximately $\pm 15^\circ$. On model 3 the angle-of-attack sting was deflected down 10° from the center line of the model in order to record higher positive values of angle of attack. Figure 7 shows a photograph of model 3 equipped with the deflected sting. Fixed wide-angle cameras and 16-millimeter motion-picture cameras recorded the launchings. The motion-picture cameras also tracked the flights.

TEST TECHNIQUE

The models were disturbed in pitch by the abrupt movement of elevons operated as elevators at preset time intervals which gave an approximately square-wave type of elevator motion. The desired aerodynamic coefficients and longitudinal-stability derivatives were obtained by analysis of the hinge moments, angle of attack, and acceleration responses resulting from these cyclic disturbances.

BASIS OF ANALYSIS

The aerodynamic coefficients, stability derivatives, and flying qualities presented in this paper were reduced from the model flight data. Specifications for satisfactory flying qualities based on military requirements and those of reference 2 have been used in this analysis. Inasmuch as these specifications are restricted to subsonic speeds and the current range of interest is in the transonic speed range, no detailed step-by-step comparison with these specifications has been attempted. Figures 8, 9, and 10 are typical portions of the recorded time histories at low supersonic, transonic, and high subsonic velocities. The variations in stability and control effectiveness through the Mach number test range can be seen in these figures by comparing the periods and amplitudes of the short-period longitudinal oscillations. A discussion of the methods used in reducing these data from the time-history records to the parameters presented in this paper is given in the appendix. The Reynolds number and the Mach number ranges of the models and of the representative full-scale airplane are shown in figure 11.

RESULTS AND DISCUSSION

Aerodynamic Coefficients and Stability Derivatives

Lift.- The lift data are presented in the form of lift-curve slope C_{L_α} for various Mach numbers (fig. 12) as obtained from two models of the same configuration but having different center-of-gravity locations and different weights. The range of angle of attack in which data were considered for determining C_{L_α} was ±15°. The lift coefficient varied linearly with angle of attack in this range. As indicated in figure 12, C_{L_α} increased approximately 25 percent from the lowest test Mach number (M = 0.88) to a Mach number of 1.00 and then decreased approximately 15 percent from M = 1.00 to M = 1.20. The increase in lift-curve slope in going through the transonic region was evident for both models. Unpublished data obtained from wind-tunnel tests of a similar model for both high subsonic and low supersonic velocities have also been plotted in figure 12.

Trim lift coefficient.- The variation of trim lift coefficient $C_{L_{trim}}$ with Mach number at different elevator deflections for model 1 is shown in figure 13(a) and for models 2 and 3, in figure 13(b). Different elevator settings for models 2 and 3 confirmed the assumption that $C_{L_{trim}}$ varied linearly with elevator deflection. These plots show an inherent

characteristic of the model configuration to trim at negative lift coefficients between Mach numbers of 0.90 and 1.08. This was due to a basic untrimmed pitching-moment coefficient C_{m_0} for the airplane at zero angle of attack and zero elevator deflection. Figure 14 shows a plot of C_{m_0} as a function of Mach number. The asymmetry of the model configuration due to the vertical tail and the upswept rear of the body would indicate an expected positive C_{m_0} which was not in accord with test results. This negative trend of figure 14, however, does agree with the data of reference 3.

Change of trim lift coefficient with respect to elevator deflection.- The rate of change in trim lift coefficient with respect to elevator deflection $C_{L_{\delta_{trim}}}$ is shown as a function of Mach number in figure 15 for models 1, 2, and 3. As would be expected, the values of $C_{L_{\delta_{trim}}}$ for model 1 with the center of gravity at 25 percent mean aerodynamic chord were larger than those of models 2 and 3 with the center of gravity at 20 percent mean aerodynamic chord. Within the Mach number range covered by the tests, $C_{L_{\delta_{trim}}}$ remained fairly constant up to $M = 0.86$ at which point an abrupt reduction from 0.049 to 0.029 occurred between $M = 0.86$ and $M = 1.00$. A further decrease from 0.029 to 0.015 occurred in $C_{L_{\delta_{trim}}}$ between $M = 1.00$ and $M = 1.28$.

Hinge-moment coefficients.- The variations of hinge-moment coefficients with angle of attack and with elevator deflection are both plotted as functions of Mach number in figure 16. The data points shown are for models 1 and 3. The theoretical points shown on the plot were calculated for a constant-chord partial-span control surface on a thin triangular wing as described in reference 4.

Calculations were made to determine the effect of elevon inertia on the hinge-moment coefficients. An extreme case showed the magnitude of the error to be negligible. Therefore, no such correction was applied to the data. Corrections were applied to eliminate the effect of phase lag between the hinge-moment coefficient and angle-of-attack curves and the effect of oscillations in elevon deflection due to angle-of-attack changes. Hinge-moment coefficients plotted as functions of angle of attack at a constant Mach number indicated that the variation was linear in the range covered by the tests ($\alpha = \pm 15^\circ$).

Figure 16 shows that C_{h_α} increases from -0.008 at $M = 0.85$ to -0.024 at $M = 1.20$. A corresponding increase from -0.015 to -0.037

is shown for C_{h_δ} between $M = 0.85$ and $M = 1.05$. Both curves indicate a gradual decrease in the low supersonic region.

The value of the basic hinge-moment coefficient at zero angle of attack and elevator deflection C_{h_0} is shown as a function of Mach number in figure 17. The basic hinge-moment coefficient C_{h_0} shows a reversal from positive to negative values at $M = 0.95$ and a tendency in the low supersonic region to return to positive values. The variation of hinge-moment coefficient with elevator deflection was assumed to be linear in the solution of C_{h_0}.

Control effectiveness.- A characteristic of the elevator used on the models can be seen in the plot of change in lift coefficient per degree of elevator deflection C_{L_δ} as a function of Mach number (fig. 18). The parameter C_{L_δ} reaches a value of 0.022 at a Mach number of 0.96 and decreases to a value of 0.010 at $M = 1.17$, a reduction of about 55 percent through this speed range. Values of C_{L_δ} are contained in reference 3 and show good agreement with the flight-test values obtained in the high subsonic and low supersonic regions.

Two more parameters of longitudinal control effectiveness for this configuration are shown in figures 19 and 20, change in trim angle of attack per degree of elevator deflection $\left(\frac{\Delta\alpha}{\Delta\delta}\right)_{trim}$, and change in pitching-moment coefficient per degree of elevator deflection C_{m_δ}, both shown as functions of Mach number. These two plots indicate an abrupt decrease in control effectiveness of the elevon between $M = 0.90$ and $M = 1.00$. This reduction is of the order of 25 percent for C_{m_δ} and 35 percent for $\left(\frac{\Delta\alpha}{\Delta\delta}\right)_{trim}$. Above a Mach number of 1.00 the curves indicate a further gradual decrease in longitudinal control effectiveness to $M = 1.28$, the highest Mach number reached by the flight tests (-0.015 at $M = 0.9$ and -0.009 at $M = 1.28$). Values of C_{m_δ} were determined for the angle-of-attack range between 10° and -8°.

The effect of center-of-gravity location is apparent in both plots by the relative displacement of results obtained from model 1 with the center of gravity at 25 percent mean aerodynamic chord and from models 2 and 3 with the center of gravity at 20 percent mean aerodynamic chord. The more rearward location of the center of gravity reduced the value of C_{m_δ} and increased the magnitude of $\left(\frac{\Delta\alpha}{\Delta\delta}\right)_{trim}$.

Longitudinal stability.- When the controls are moved up and down in
a square-wave type of motion, corresponding changes are produced in angle
of attack and normal acceleration. The stability of the configuration
is indicated by the period and the rate of decay of the short-period lon-
gitudinal oscillation when the controls are held fixed between pulses.

The values of the period of the short-period oscillation induced by
this abrupt control movement as determined from the time-history records
are presented in figure 21 to show the variation of the period with Mach
number for the models. The period decreased, a stability increase being
indicated, from a Mach number of 0.75, the lower test limit, to approx-
imately M = 0.95. Above this speed the period continued to decrease
but at a much more gradual rate up to M = 1.28, the upper limit of the
speed range covered by the flight tests. The period for model 1 was
greater than that for models 2 and 3 throughout its test range as would
be expected since the center of gravity of model 1 was 5 percent of the
mean aerodynamic chord behind the center-of-gravity location for models 2
and 3.

The static-longitudinal-stability parameter in the form of the change
in pitching-moment coefficient with respect to a change in angle of
attack C_{m_α} is shown as a function of Mach number in figure 22 for C_L
values between ± 0.30. The determination of C_{m_α} involved the use of
the period of the short-period oscillations as a primary factor. The
value of C_{m_α} increased from a minimum of -0.0095 at M = 0.85 to a
maximum of -0.0162 at M = 1.15 for models 2 and 3 with the center of
gravity at 20 percent mean aerodynamic chord. An investigation of the
change in C_{m_α} due to a 5-percent change in center-of-gravity location
shows that C_{m_α} for model 1 is lower than would be expected from a com-
parison with models 2 and 3. Data concerning the evaluation of C_{m_α}
were carefully rechecked and there were indications that the seemingly low
values of C_{m_α} were due to accumulative errors within the accuracy of
determining the physical characteristics used to calculate this parameter.

Figure 23, a plot of aerodynamic-center position against Mach number,
also indicates the variation of the static longitudinal stability. The
aerodynamic center moved very gradually from a minimum of 42 percent of
the mean aerodynamic chord at a Mach number of 0.80 to a maximum of
54 percent of the mean aerodynamic chord at a Mach number of 1.15. The
aerodynamic-center positions for model 1, however, were $2\frac{1}{2}$ percent of
the mean aerodynamic chord ahead of models 2 and 3. The more forward
aerodynamic-center locations for model 1 were a result of the low values
of C_{m_α} obtained for this model. This difference, however, is within
the accuracy of aerodynamic-center location usually obtained from flight
and wind-tunnel data.

The three parameters discussed in the preceding paragraphs (period, C_{m_α}, and aerodynamic-center position) show that the static longitudinal stability of this configuration increased through the transonic region from a minimum value at about $M = 0.82$ to a maximum value at $M = 1.15$.

A qualitative evaluation of the dynamic stability may be made by inspection of the damping of the short-period oscillation induced by the abrupt control movement. Damping is represented by the parameter $T_{1/2}$, the time required to damp to one-half amplitude, and is presented in figure 24 as it varies with Mach number. Since the flight-test models were not dynamic-scale models, the results presented in figure 24 are applicable to the full-scale airplane only after corrections are applied. Models 2 and 3 with the center of gravity at 20 percent mean aerodynamic chord showed more rapid damping characteristics than model 1 with its center of gravity at 25 percent mean aerodynamic chord.

The total damping factor $C_{m_{\frac{\dot\theta\bar c}{2V}}} + C_{m_{\frac{\dot\alpha\bar c}{2V}}}$, which is a measure of the dynamic stability of the configuration expressed nondimensionally, is presented in figure 25 as a function of Mach number. Model 1 with the more rearward center-of-gravity location indicated less tendency to damp throughout the flight-test speed range than did models 2 and 3.

It will be noted that there is considerable scatter in the damping data. This type of scatter may also be expected for full-scale airplane conditions inasmuch as the present data were obtained in free flight and all the aerodynamic factors that affect damping were properly integrated into the motion of the models.

Directional stability.- Only models 1 and 2 were instrumented to obtain transverse accelerations. Model 2 apparently had some directional asymmetry that caused it to develop a small positive side force throughout the flight. This effect approximately doubled at Mach numbers below 0.90. Model 1 did not exhibit any such consistent side-force variation, the side forces on model 1 resulting from an occasional disturbance. Neither model showed divergence nor continuous oscillations; thus, positive directional stability was indicated.

Flying Qualities

Longitudinal trim characteristics.- The longitudinal trim characteristics of the configuration are as follows:

Trim angle of attack: The angle of attack for trimmed level flight required for this configuration is presented as a function of Mach number in figure 26. Curves are shown for center-of-gravity locations at

20 and 25 percent of the mean aerodynamic chord for both sea-level flight and flight at an altitude of 40,000 feet. The trim angle of attack shows a consistent small decrease with increasing speed except in the region between $M = 0.90$ and $M = 0.95$.

Control position for trim: The characteristics of the elevator control in level flight are presented in figure 27 in the form of the variation of the elevator position required for trim with Mach number. Control-position trim change is manifested between a Mach number of 0.87 and 0.95 at sea level and 40,000 feet. The control-position trim change is a function of variation of out-of-trim pitching moment with Mach number, change in control effectiveness, and movement of the neutral point. The resultant change in trim, a tucking-under tendency, appears to be of moderate magnitude. For example, at 40,000 feet a maximum up-elevator angle of about 5° is required for trim at a Mach number of 0.95.

An evaluation of the stick-fixed maneuver point in the Mach number range between 0.80 and 1.20 indicated that the point is well behind the most rearward center-of-gravity position and the requirements for maneuvering stability are met.

Figures 28 to 31 present the control positions required for maneuvering at various accelerations as functions of Mach number. Figures 28 and 29 are curves for sea level and 40,000 feet, respectively, with the center of gravity located at 25 percent mean aerodynamic chord. Figures 30 and 31 are also curves for sea level and 40,000 feet, respectively, but with the center of gravity located at 20 percent mean aerodynamic chord. For example, figure 29 shows that at a Mach number of 1.20 an up-elevator deflection of 10° would produce 5g normal acceleration at 40,000 feet with the center of gravity located at 25 percent mean aerodynamic chord.

Longitudinal control forces: The elevator control force required for trim in straight and level flight at various Mach numbers is presented in figure 32 for sea-level flight and in figure 33 for flight at 40,000 feet. The stick force per g is presented in figure 34 as a function of Mach number. The stick forces are based on a conventional airplane configuration with 2° of elevator deflection for 1 inch of stick movement. Therefore, these data indicate the power required of a control-boost system with no balancing and trimming devices. For example, with the center of gravity at 25 percent mean aerodynamic chord at a Mach number of 1.20 the stick force per g based on measured hinge moments is about 900 pounds per g.

The variation of elevator control force for trim with Mach number (fig. 32) indicated that pull forces were required at all speeds below the trim speed and push forces were required at all speeds above the trim speed within the range of Mach numbers from 0.95 to 1.20. The opposite

is true for Mach numbers from 0.80 to 0.95, but the elevator angle for
trim in this range of Mach number increases with increasing Mach number.
Thus, the stick force would be in the correct sense with respect to stick
movement throughout the transonic region.

The elevator hinge-moment data obtained for model 1 indicate a
force reversal at high angles of attack ($\alpha \geqq 15^\circ$) at Mach numbers
below 0.90. Model 2, which flew at angles of attack of about 7° at
M = 0.90, did not show a hinge-moment reversal but did indicate hinge
moments near zero.

Longitudinal control effectiveness.- The variation with Mach number
of the normal acceleration produced per unit of elevator deflection
$\left(\dfrac{\Delta a_n}{\Delta \delta}\right)_{trim}$ is presented in figure 35. At sea level a large variation in
elevator effectiveness was apparent from subsonic to low supersonic
speeds with minimum effectiveness occurring at a Mach number of 1.06 for
model 1 with the center-of-gravity location at 25 percent mean aerodyna-
mic chord and at a Mach number of 0.98 for models 2 and 3 with the
center-of-gravity location at 20 percent mean aerodynamic chord. Suffi-
cient control for maneuvering is available as indicated by the fact that
10° elevator deflection will produce 5g acceleration at a Mach number
of 1.20 at 40,000 feet with the center of gravity located at 25 percent
mean aerodynamic chord.

Dynamic stability.- The characteristics of the stick-fixed short-
period longitudinal oscillations are presented in figures 36 to 38 for a
full-scale configuration. Military specifications for stability-and-
control characteristics of airplanes require that the short-period
dynamic oscillation of normal acceleration produced by moving and quickly
releasing the elevator shall be damped to 1/2 amplitude in 1 cycle (based
on free controls). The damping characteristics for the full-scale con-
figuration have been evaluated for the control-fixed condition although
there is a slight oscillation in the control position due to hinge-moment
effect which is apparent in figures 8 to 10. The fixed-control charac-
teristics would probably dictate the behavior of this airplane since it
would require some kind of control-boost system to aid the pilot in over-
coming the extremely large stick forces encountered in maneuvering. Fig-
ure 36, which gives the cycles required to damp to 1/2 amplitude as a
function of Mach number at sea level and at a 40,000-foot altitude, would
meet such a requirement for both conditions.

Figure 37 shows the time required for the short-period oscillations
of the full-scale airplane to damp to half amplitude as a function of

Mach number at sea level and 40,000 feet. As can be seen from this figure, $T_{1/2_a}$ decreases through the transonic region and reaches a relatively constant value at about M = 1.20. Period as a function of Mach number is shown in figure 38 for sea level and 40,000 feet. Both the time to damp to half amplitude and period indicate increasing stability for the configuration with increasing Mach number in the transonic and low supersonic speed range.

CONCLUSIONS

From the results of a flight investigation made to evaluate the aerodynamic characteristics and flying qualities of models of a tailless triangular-wing airplane configuration, the following general conclusions are indicated for the Mach number range between 0.75 and 1.28:

Aerodynamic Characteristics

1. The lift coefficients varied linearly in the angle-of-attack test range of ±15°. The lift-curve slope C_{L_α} varied from 0.045 at a Mach number M of 0.88 to a maximum of 0.055 at a Mach number of 1.0 and then decreased to 0.0475 at a Mach number of 1.20.

2. The hinge-moment coefficient per degree of angle of attack increased 200 percent between M = 0.85 and M = 1.20; whereas the hinge-moment coefficient per degree of elevator showed a corresponding rise of 150 percent between M = 0.85 and M = 1.05. Both of these values showed a gradual decrease in the low supersonic region.

3. The elevator effectiveness decreased by approximately 40 percent from a Mach number of 0.9 to 1.25. For example, with the center of gravity at 20 percent mean aerodynamic chord, the rate of change of pitching-moment coefficient with elevator deflection C_{m_δ} at a Mach number of 0.9 was -0.015 and at a Mach number of 1.25 was -0.009.

4. The configuration tested possessed static longitudinal stability throughout the Mach number range covered by these flight tests. The value of C_{m_α} (rate of change of pitching-moment coefficient with angle of attack) increased from a minimum at M = 0.80 to a maximum at M = 1.15 with the center of gravity at 20 percent mean aerodynamic chord.

5. The aerodynamic center moved very gradually from a minimum of 42 percent of the mean aerodynamic chord at a Mach number of 0.80 to a maximum of 54 percent of the mean aerodynamic chord at a Mach number of 1.15.

6. The damping parameters and coefficients indicated that the configuration possessed dynamic longitudinal stability throughout the test speed range.

7. The models exhibited directional stability throughout the angle-of-attack and speed ranges of the tests.

Flying Qualities

1. There is ample control for trim in level flight at sea level or at altitude. At 40,000 feet a maximum up-elevator angle of about 5° is required for trim at a Mach number of 0.96. The transonic trim change, a tucking-under tendency, appears to be mild.

2. The elevator control remains effective in changing lift or angle of attack over the entire speed range. The effectiveness of the elevator in changing angle of attack, however, is reduced to about half of its subsonic value at supersonic speeds. This change of effectiveness occurs gradually.

3. With the center of gravity at 25 percent mean aerodynamic chord the normal acceleration produced per degree elevator deflection is such that about 10° up-elevator deflection is required to produce a 5g acceleration at 40,000 feet at a Mach number of 1.2. The corresponding stick force per g based on the measured hinge moments is about 900 pounds per g, a figure which gives an indication of the power required of a control-boost system.

4. According to military requirements, the damping of the short-period longitudinal oscillation is adequate over the speed range for both sea-level conditions and at an altitude of 40,000 feet.

Langley Aeronautical Laboratory,
    National Advisory Committee for Aeronautics,
        Langley Field, Va., December 7, 1949.

APPENDIX

REDUCTION OF DATA AND METHODS OF ANALYSIS

Reduction of Data

Mach number.- The total pressures obtained from the telemeter records were reduced to Mach number by use of the following equations:

Subsonic:

$$\frac{H}{p} = \left(1 + \frac{\gamma - 1}{2} M^2\right)^{\frac{\gamma}{\gamma-1}} \tag{1}$$

Supersonic:

$$\frac{H}{p} = \frac{\left(\frac{\gamma + 1}{2} M^2\right)^{\frac{\gamma}{\gamma-1}}}{\left(\frac{2\gamma}{\gamma + 1} M^2 - \frac{\gamma - 1}{\gamma + 1}\right)^{\frac{1}{\gamma-1}}} \tag{2}$$

where p, free-stream static pressure, was obtained from the reference static-pressure record in conjunction with radiosonde data. Models 1 and 3 reached a maximum altitude of 4,000 feet while model 2 attained a maximum of 4,700 feet. The Doppler velocimeter radar unit served as an independent check of the Mach number obtained by reduction of the total and reference static pressures.

Angle of attack.- Since angle-of-attack data were measured at a point some distance ahead of the center-of-gravity location, it was necessary to correct these data for flight-path curvature and angular velocity as described in reference 1. The following equation was used:

$$\alpha = \alpha_i + \frac{d}{V}\left(1,844 \frac{a_n}{g} \frac{1}{V} + \frac{d\alpha_i}{dt}\right) \tag{3}$$

Control position.- Prior to the flight test of each model a static hinge-moment calibration of the control system was conducted to determine the amount of twist that would be encountered in the elevons and control linkage under aerodynamic loads. The elevons were loaded at two spanwise stations and readings were taken at five points to measure the amount of twist or deflection induced. Control-position data recorded during flight were corrected by the calibration obtained from the static test.

Analysis of Aerodynamic Coefficients and Derivatives

The methods of analysis used herein apply to the free oscillation resulting from a step function disturbance. The disturbance was created by an approximately square-wave type of motion of the elevators moved abruptly between limit stops. The complete derivation of the equations used will not be given herein but the basic equations of motion are as follows:

$$Vm(\dot{\theta} - \dot{\alpha}) = \left(C_{L_\alpha}\alpha + C_{L_\delta}\delta\right)57.3qS \tag{4}$$

$$I_Y\ddot{\theta} = \left(C_{m_\alpha}\alpha + C_{m_{\dot{\alpha}}}\dot{\alpha} + C_{m_{\dot{\theta}}}\dot{\theta} + C_{m_\delta}\delta\right)57.3qS\bar{c} \tag{5}$$

In order to simplify the analysis and to permit the determination of equations for the more important aerodynamic derivatives, a number of assumptions are necessary. It is assumed that, during the time interval over which each calculation is made, the forward velocity is constant and the aerodynamic forces and moments vary linearly with the variables α, δ, and θ.

Figure 39 is a schematic plot showing a typical record of the control position and lift-coefficient responses following step deflections of the aircraft control surfaces. At least three complete peaks of each disturbance were necessary to obtain the trim lines shown in the oscillations. Where three complete peaks were not present, sufficient accuracy in placing the trim line could not be ascertained and such data carried little weight in the analysis.

Lift-curve slope.- Several methods were tried for determining the lift-curve slope with respect to angle of attack. The most expeditious method found was to measure the instantaneous slopes $\frac{dC_L}{dt}$ and $\frac{d\alpha}{dt}$ at a given Mach number. Care was exercised in using only the portions of the lift coefficient and angle-of-attack time-history curves where the slopes could be accurately ascertained. The effect of lift due to the flexibility of the elevator was eliminated by correcting $\frac{dC_L}{dt}$ for the lift due to the deviation of the elevator deflection from a fixed value at an instantaneous time. The following relation exists:

$$C_{L_\alpha} = \frac{\Delta C_{L_{2-1}} - C_{L_\delta}\Delta\delta_{2-1}}{\Delta\alpha_{2-1}} \tag{6}$$

where $\Delta C_{L_{2-1}}$ is the change in C_L between C_{L_2} and C_{L_1} taken over a relatively straight portion of the lift time history as indicated in

figure 39 and $\Delta\delta_{2-1}$ and $\Delta\alpha_{2-1}$ are incremental changes in δ and α over the same time interval. The value of C_{L_δ} used in this equation was a first approximation. Successive approximations and evaluations were unnecessary.

After the corrected value of C_{L_α} was determined, it was then possible to determine an exact value for C_{L_δ}, the lift-curve slope due to the elevons, from the portions of the time histories where the controls were moving from one extreme position to the other. The following relation exists:

$$C_{L_\delta} = \frac{\left(\Delta C_{L_{2-1}}\right)_{trim} - C_{L_\alpha}\left(\Delta\alpha_{2-1}\right)_{trim}}{\left(\Delta\delta_{2-1}\right)_{trim}} \tag{7}$$

The values of α, δ, and C_L are trim values as illustrated in figure 39. Although $\left(\Delta\alpha_{2-1}\right)_{trim}$ is not included in the illustration, it would be obtained in the same manner.

The variation of trim lift coefficient with respect to elevator deflection $C_{L_{\delta trim}}$ was found by the same method used to find C_{L_δ}. The equation is

$$C_{L_{\delta trim}} = \frac{\left(\Delta C_{L_{2-1}}\right)_{trim}}{\left(\Delta\delta_{2-1}\right)_{trim}} \tag{8}$$

and the quantities used are again illustrated in figure 39.

The trim lift coefficients $C_{L_{trim}}$ corresponding to the trim elevator deflections encountered in the tests were plotted against Mach number in figure 13. Trim lift coefficients for elevator settings between $\pm 5^\circ$ were derived by using a linear relation between lift coefficient and elevon deflection at a constant Mach number.

Pitching moments.- The basic untrimmed pitching-moment coefficient C_{m_0} was calculated from the conventional moment-coefficient equation solved for C_{m_0} as follows:

$$C_{m_0} = -C_{m_\alpha}\alpha_{trim} - \left(C_{m_\delta}\right)_{\alpha=K}\delta_{trim} \tag{9}$$

The derivatives C_{m_α} and C_{m_δ} were considered linear in the range of the tests. The second term was eliminated by taking values of $C_{L_{trim}}$ for an elevator deflection of $0°$ and dividing the first term by C_{L_α} to make C_{m_0} a function of the trim lift coefficient, or

$$C_{m_0} = -C_{m_\alpha}\alpha_{trim_{\delta=0}} \tag{10}$$

and

$$C_{m_0} = -\frac{C_{m_\alpha}}{C_{L_\alpha}}\left(C_{L_{trim}}\right)_{\delta=0} \tag{11}$$

The values of C_{m_α} were obtained as described in the section on longitudinal stability.

Hinge moments.- Hinge-moment data were reduced to coefficient form and plotted directly against angle of attack for both up and down elevator deflection to obtain an approximate value of C_{h_δ}. This value was used in conjunction with the change in δ due to changes in α to correct the values of the total hinge moment for constant elevator deflection as follows:

$$\left(C_h\right)_{\delta=K} = C_h + \Delta\delta C_{h_\delta} \tag{12}$$

The values obtained were plotted as functions of time as were the values of angle of attack. A method was derived to eliminate the effect of phase lag between the two variables. Constant values of C_h were chosen on each side of an oscillation peak and a mean value of α corresponding to the constant value of C_h was determined analytically and graphically. Finally, the corrected values of C_h and α were plotted for up and down elevator to determine C_{h_α} and C_{h_δ}. There were indications that these values were linear and C_{h_0}, the hinge-moment coefficient at zero angle of attack and elevator, was determined by direct interpolation.

Control effectiveness.- The variation of trim angle of attack with elevator deflection $\left(\frac{\Delta\alpha}{\Delta\delta}\right)_{trim}$ was found by using the method illustrated by figure 39 and the following equation:

$$\left(\frac{\Delta\alpha}{\Delta\delta}\right)_{trim} = \frac{\left(\Delta\alpha_{2-1}\right)_{trim}}{\left(\Delta\delta_{2-1}\right)_{trim}} \tag{13}$$

The resulting values were used to obtain the control-effectiveness parameter C_{m_δ} at a constant angle of attack in the following manner:

$$\left(C_{m_\delta}\right)_{\alpha=K} = -C_{m_\alpha}\left(\frac{\Delta\alpha}{\Delta\delta}\right)_{trim} \tag{14}$$

The solution of C_{m_α} is presented in the discussion of longitudinal stability which follows.

Longitudinal stability.- Evaluations of the longitudinal stability were obtained by analysis of the short-period oscillations induced by the abrupt control movements and shown in the angle-of-attack curves in the time histories. The solution of C_{m_α}, the static longitudinal stability derivative, is obtained from the following equation as derived from the simultaneous solution of the two equations of motion:

$$C_{m_\alpha} = -\frac{I_Y}{qS\overline{c}}\left[\frac{4\pi^2}{P^2} + \left(\frac{0.693}{T_{1/2}}\right)^2\right] \tag{15}$$

A correction was applied to C_{m_α} to eliminate the effect of elevon flexibility and the second-order effects from the two-degrees-of-freedom method of analysis were neglected since they constituted less than 0.5 percent of the results.

The periods of the short-period oscillation P were read from the time-history curves and the time to damp the amplitudes to one-half magnitude was determined by the use of the following formula:

$$T_{1/2} = \frac{0.693\ P}{2\ \log_e\left(A_1/A_2\right)} \tag{16}$$

where A_1 and A_2 were successive amplitudes above and below the neutral axis of the angle-of-attack time history at the point where $T_{1/2}$ was sought.

The quantities C_{m_α} and C_{L_α}, corrected for the effect of elevator oscillations, were used in conjunction with the model center-of-gravity

locations to determine the aerodynamic-center positions in percentages of the mean aerodynamic chord. Reference 5 presents the following relation:

$$\text{Aerodynamic center} = \text{Center of gravity} - \left(\frac{dC_{m_\alpha}}{dC_{L_\alpha}}\right)_{\text{corrected}} \tag{17}$$

The dynamic-longitudinal-stability data were reduced to the form of $C_{m_{\frac{\dot\theta \bar c}{2V}}} + C_{m_{\frac{\dot\alpha \bar c}{2V}}}$ by the following equation derived from the simultaneous solution of the two equations of motion:

$$C_{m_{\frac{\dot\theta \bar c}{2V}}} + C_{m_{\frac{\dot\alpha \bar c}{2V}}} = -\frac{8I_Y}{\rho V S \bar c^2}\left(\frac{0.693}{T_{1/2}} - \frac{57.3 C_{L_\alpha}\rho V S}{4m}\right) \tag{18}$$

Flying-Qualities Analysis

Variation with Mach number of the control position required for trim in level flight.- The trim lift coefficient $C_{L_{\text{trim}}}$ for 0° elevator deflection was obtained by plotting values of C_L corresponding to constant positive and negative elevator deflections against Mach number, and the variations were considered to be linear in the test range. These values were taken from the trim values of C_L and δ obtained from the time-history data of the flight tests of the three models. The value of $C_{L_{\text{trim}}}$ for $\delta = 0^\circ$ was obtained by interpolation. Values of C_L for level flight for the full-scale airplane were obtained from the relation $\left(C_L\right)_{\text{lg}} = \frac{W/S}{q}$. The difference between $\left(C_L\right)_{\text{lg}}$ for straight and level flight and $C_{L_{\text{trim}}}$ for $\delta = 0^\circ$ was divided by $C_{L_{\delta_{\text{trim}}}}$ to give δ for straight and level flight for various Mach numbers.

$$\delta_{\text{trim}} = \frac{\left(C_L\right)_{\text{lg}} - \left(C_{L_{\text{trim}}}\right)_{\delta=0^\circ}}{C_{L_{\delta_{\text{trim}}}}} \tag{19}$$

Elevator control force for trim against Mach number.- A value of deflection of elevator per inch of stick movement for a high-speed fighter-type airplane was assumed to be

$$\frac{\delta}{x} = 2^\circ \text{ per inch}$$

Values of hinge moment were obtained from the time-history plots of models for corresponding δ_{trim} values against Mach number. The method for determining trim lines was the same as in figure 39. The value of $\left(\dfrac{\Delta H}{\Delta \delta}\right)_{trim}$ was obtained from

$$\left(\frac{\Delta H}{\Delta \delta}\right)_{trim} = \frac{\left(H_2 - H_1\right)_{trim}}{\left(\delta_2 - \delta_1\right)_{trim}} = \frac{\left(\Delta H_{2-1}\right)_{trim}}{\left(\Delta \delta_{2-1}\right)_{trim}} \qquad (20)$$

At a given Mach number a value of hinge moment was read at a given elevator deflection and corrected to the δ_{trim} for straight and level flight at sea-level conditions by

$$H_{\delta_{trim}} = H_1 - \left(\delta_1 - \delta_{trim}\right)\left(\frac{\Delta H}{\Delta \delta}\right)_{trim} \qquad (21)$$

If the hinge moment for δ_{trim} for straight and level flight at sea-level conditions is known, the elevator control force is obtained by

$$F = \frac{H}{57.3} \frac{\delta}{x} \qquad (22)$$

where H has been corrected to full scale.

<u>Change in normal acceleration for a corresponding change in elevator deflection</u> $\left(\dfrac{\Delta a_n}{\Delta \delta}\right)_{trim}$ <u>against Mach number.-</u> In order to obtain the change in normal acceleration for a corresponding change in elevator deflection against Mach number the values of C_L for level flight for various Mach numbers were divided by $C_{L_{\delta_{trim}}}$ (eq. (8)) so that for 1 g the reciprocal of $\left(\dfrac{\Delta a_n}{\Delta \delta}\right)_{trim}$ is

$$\Delta \delta = \frac{\left(C_L\right)_{1g}}{C_{L_{\delta_{trim}}}} \qquad (23)$$

<u>Stick force per g against Mach number.-</u> The change in elevator deflection required for a change in normal acceleration of 1 g, reciprocal of $\left(\dfrac{\Delta a_n}{\Delta \delta}\right)_{trim}$, was multiplied by $\left(\dfrac{\Delta H}{\Delta \delta}\right)_{trim}$ (eq. (20)) to obtain the

change in hinge moment required for a change in normal acceleration of 1 g. Then, for $\frac{\Delta F}{g}$ in pounds per g,

$$\frac{\Delta F}{g} = \left(\frac{\Delta \delta}{g}\right)_{trim} \left(\frac{\Delta H}{\Delta \delta}\right)_{trim} \frac{\delta}{x} \frac{1}{57.3} \tag{24}$$

Dynamic stability.- The dynamic stability of the airplane in terms of period and damping of the short-period longitudinal oscillations was determined from the oscillations of the model corrected to full-scale conditions.

The correction factors were determined from a two-degree-of-freedom method of analysis of the motion which assumes no changes in forward speed during the oscillation. The period of the oscillation for the airplane in terms of period for the model was obtained from a ratio of the C_{m_α} equations for the two as

$$P_a = P_m \frac{a_m}{a_a} \sqrt{\frac{I_{Y_a}}{S_a \bar{c}_a} \frac{S_m \bar{c}_m}{I_{Y_m}} \frac{\rho_m}{\rho_a}} \tag{25}$$

The time to damp to one-half amplitude for the airplane was determined by the following relationship:

$$C_{m_{\frac{\dot\theta \bar{c}}{2V}}} + C_{m_{\frac{\dot\alpha \bar{c}}{2V}}} = \frac{-8 I_Y}{\rho a M S \bar{c}^2}\left(\frac{0.693}{T_{1/2}} - \frac{57.3 C_{L_\alpha} \rho a M S}{4m}\right) \tag{26}$$

and equated for model and airplane as follows:

$$\frac{0.693}{T_{1/2_a}} = -\frac{57.3 C_{L_\alpha} \rho_a a_a M S_a}{4}\left(-\frac{1}{m_a} + \frac{I_{Y_m} \bar{c}_a^2}{I_{Y_a} m_m \bar{c}_m^2}\right) + \left(\frac{I_{Y_m} a_a \rho_a S_a \bar{c}_a^2}{I_{Y_a} a_m \rho_m S_m \bar{c}_m^2}\right)\left(\frac{0.693}{T_{1/2_m}}\right) \tag{27}$$

Flying-qualities specifications require that the short-period oscillations damp to one-half amplitude in one complete cycle. This value was determined from the relation

$$C_{1/2_a} = \frac{T_{1/2_a}}{P_a} \tag{28}$$

for the representative full-scale airplane.

REFERENCES

1. Mitchell, Jesse L., and Peck, Robert F.: An NACA Vane-Type Angle-of-Attack Indicator for Use at Subsonic and Supersonic Speeds. NACA TN 3441, 1955. (Supersedes NACA RM L9F28a.)

2. Gilruth, R. R.: Requirements for Satisfactory Flying Qualities of Airplanes. NACA Rep. 755, 1943. (Supersedes NACA ACR, Apr. 1941.)

3. Lawrence, Leslie F., and Summers, James L.: Wind-Tunnel Investigation of a Tailless Triangular-Wing Fighter Aircraft at Mach Numbers From 0.5 to 1.5. NACA RM A9B16, 1949.

4. Tucker, Warren A., and Nelson, Robert L.: Theoretical Characteristics in Supersonic Flow of Two Types of Control Surfaces on Triangular Wings. NACA Rep. 939, 1949. (Supersedes NACA TN's 1600 and 1601 by Tucker and TN 1660 by Tucker and Nelson.)

5. Phillips, William H.: Appreciation and Prediction of Flying Qualities. NACA Rep. 927, 1949. (Supersedes NACA TN 1670.)

TABLE I

PHYSICAL CHARACTERISTICS OF THE MODEL OF A TAILLESS TRIANGULAR-WING AIRPLANE

CONFIGURATION AND OF A REPRESENTATIVE FULL-SCALE CONFIGURATION

	Model	Full-scale configuration
Wing:		
Area (fuselage included), sq ft	6.25	425
Span, ft	3.80	31.33
Aspect ratio	2.31	2.31
Mean aerodynamic chord, ft	2.19	18.08
Sweepback of leading edge, deg	60	60
Dihedral (relative to mean thickness line), deg . . .	0	0
Taper ratio (Tip chord/Root chord)	0	0
Airfoil section	NACA $65_{(06)}$-006.5	NACA $65_{(06)}$-006.5
Vertical tail:		
Area (outside of fuselage), sq ft	0.81	76.0
Height (outside of fuselage), ft	0.97	9.31
Aspect ratio . . . . ,	2.31	2.31
Sweepback of leading edge, deg	60	60
Taper ratio (Tip chord/Root chord)	0	0
Airfoil section	NACA $65_{(06)}$-006.5	NACA $65_{(06)}$-006.5
Elevon:		
Type	Plain flap	-----
Area (aft of hinge line, one) sq ft	0.51	38.3
Span (at trailing edge of wing, one) ft	1.78	-----
Chord (hinge line to trailing edge), ft	0.37	-----

TABLE II

WEIGHT AND BALANCE DATA FOR MODELS 1, 2, AND 3 AND FULL-SCALE

TAILLESS TRIANGULAR-WING CONFIGURATION

Configuration	Weight, lb	Wing loading, lb/sq ft	Center-of-gravity position, percent M.A.C.	Moment of inertia, I_Y, slug-ft^2
Rocket fuel included in models				
Model 1	188.00	30.1	29.7	17.52
Model 2	189.75	30.4	24.0	17.89
Model 3	186.75	29.9	24.1	18.76
Models without rocket fuel				
Model 1	182.50	29.2	25.0	16.65
Model 2	184.25	29.5	20.0	17.10
Model 3	181.25	29.0	20.0	17.93
Full-scale configuration (normal gross weight)				
Full scale	11,600	27.3	25.0	27,283
Full scale	11,600	27.3	20.0	27,283
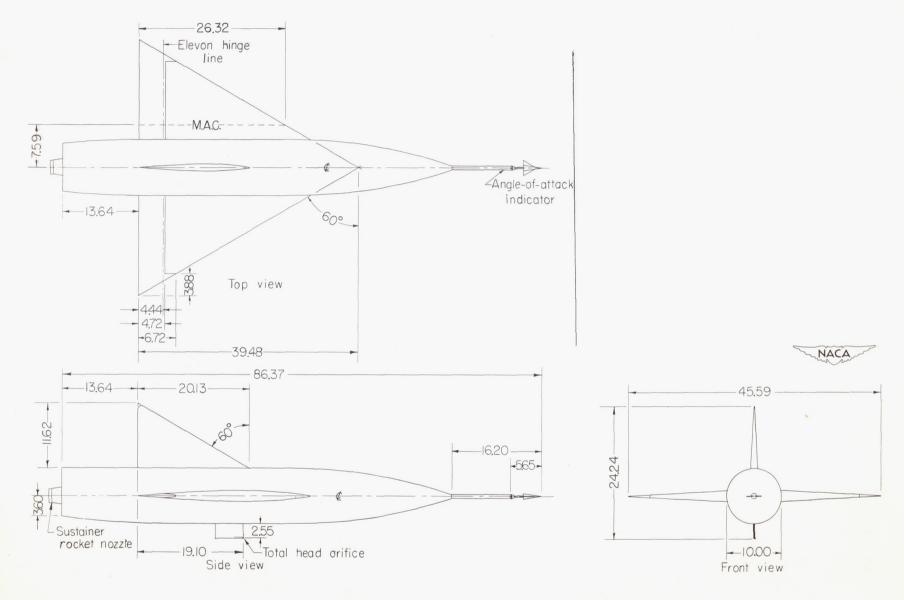
Figure 1.- Three-view drawing of the rocket-powered
flight model. All dimensions are in inches.

Figure 2.- Side view of model.
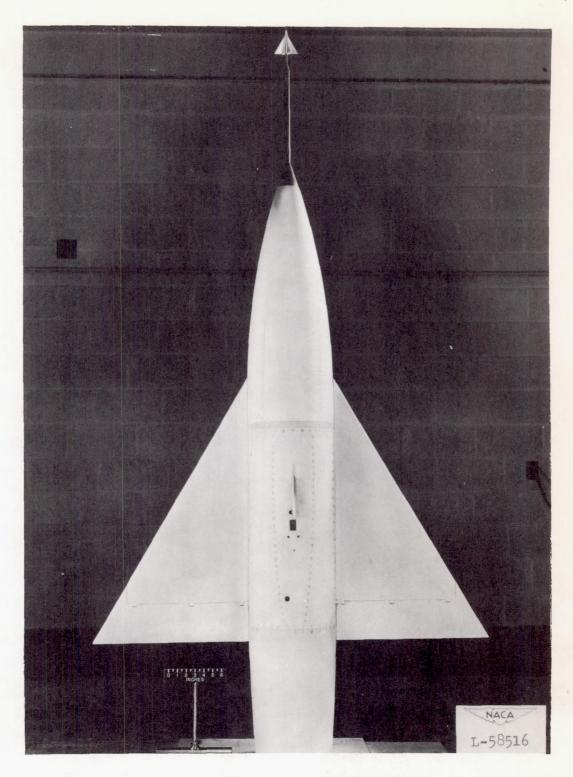
Figure 3.- Bottom view of model.

Figure 4.- Model-booster combination on launcher.

L-57682
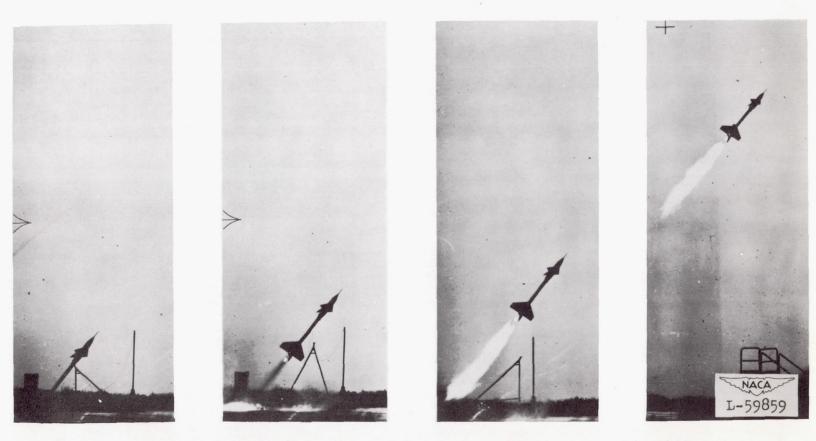
Figure 5.- Photographs of launching of the model-booster combination.

RADIO FREQUENCY
TRANSMITTER

MODULATOR

TOTAL HEAD PRESSURE
PICKUP

INTERNAL BATTERY
BOX

TRANSVERSE
ACCELEROMETER PICKUP

AIR ACCUMULATOR

CONTROL POSITION
PICKUP

PICK-UP OSCILLATORS

NORMAL
ACCELEROMETER PICKUP

LONGITUDINAL
ACCELEROMETER PICKUP

AIR PRESSURE
SWITCHING MOTOR

AIR SERVO

ELEVON HINGE-MOMENT
PICKUP

ELEVON ACTUATING ARM

NACA

L-58517
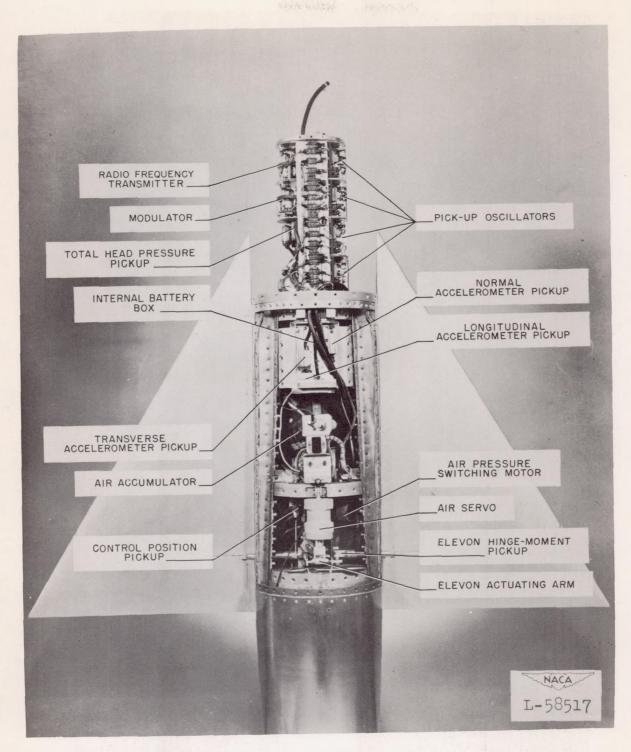
Figure 6.- Instrumentation arrangement on a typical model.
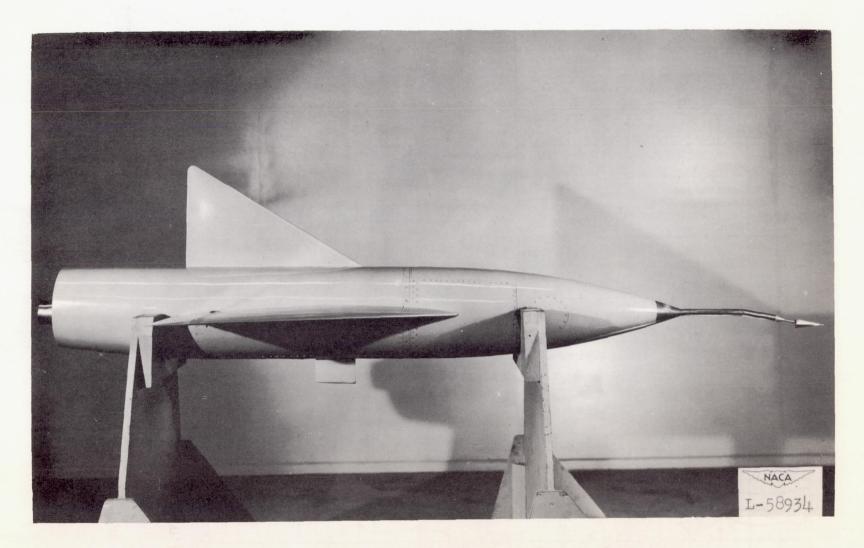
Figure 7.- Side view of model showing deflected angle-of-attack sting.
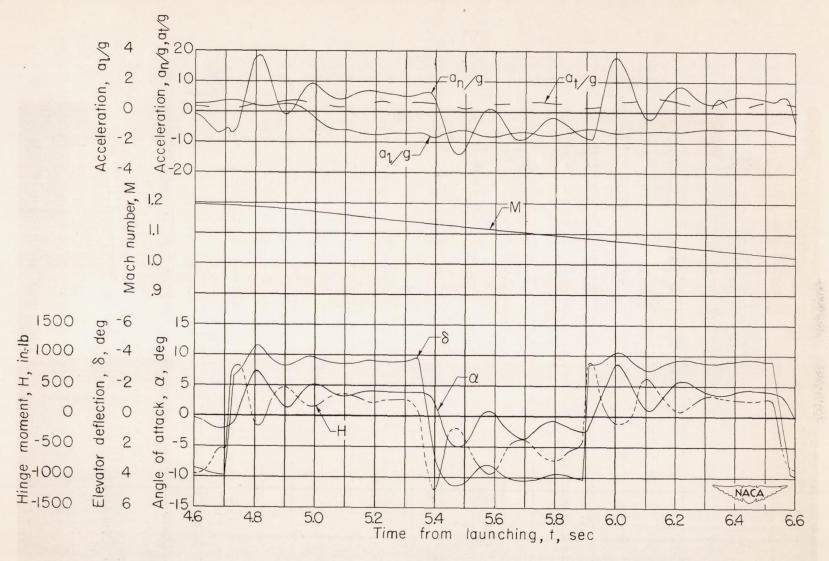
Figure 8.- Typical section of a time history at low supersonic speeds.
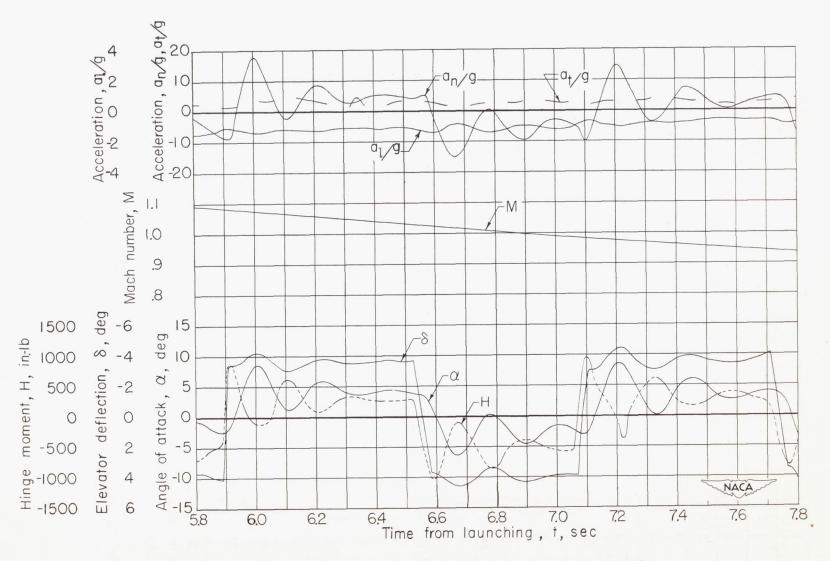
Figure 9.- Typical section of a time history at transonic speeds.
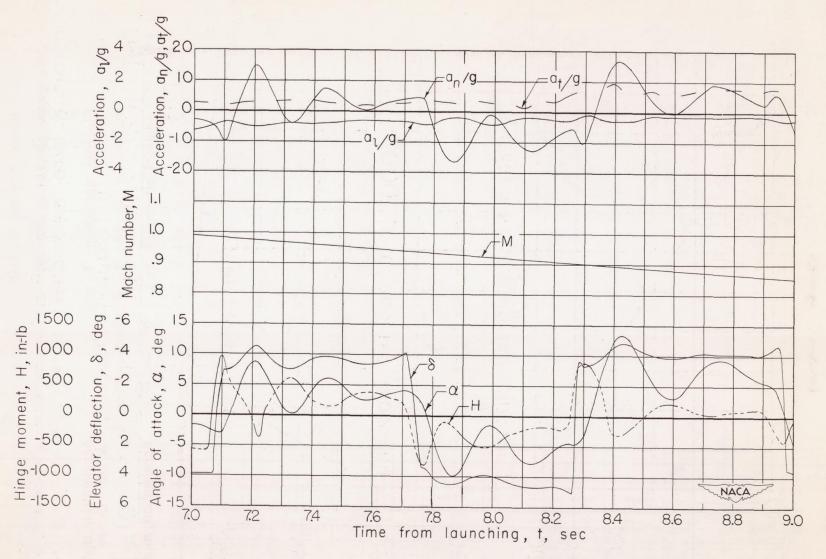
Figure 10.- Typical section of a time history at high subsonic speeds.
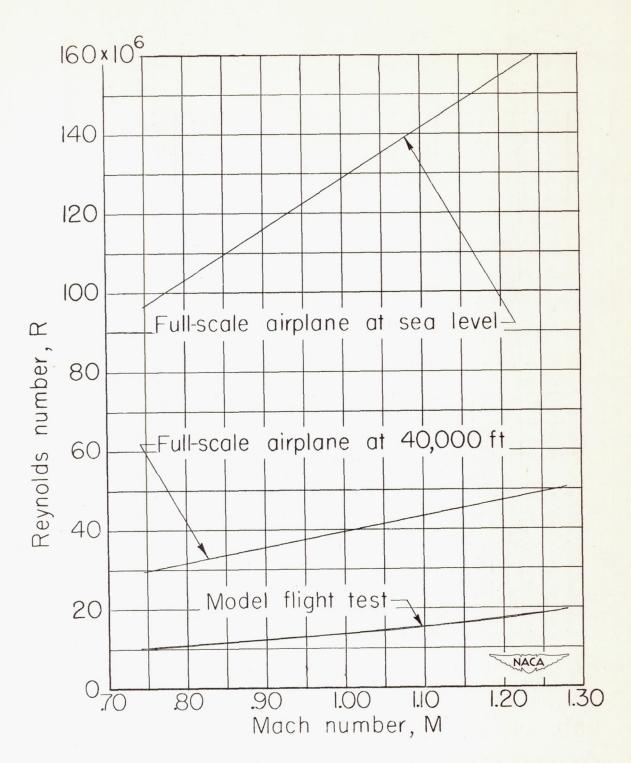
Figure 11.- Variation of Reynolds number with Mach number for flight of
the full-scale airplane at two altitudes and for flight model test
data.
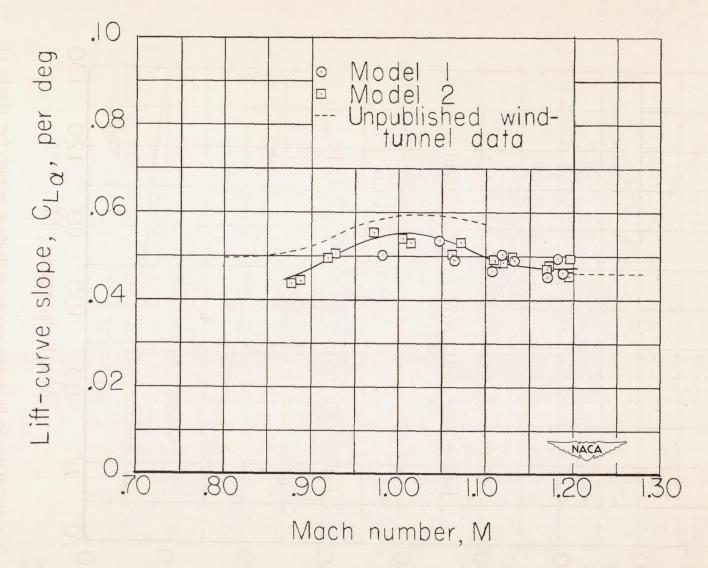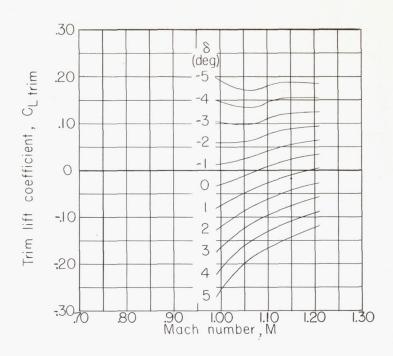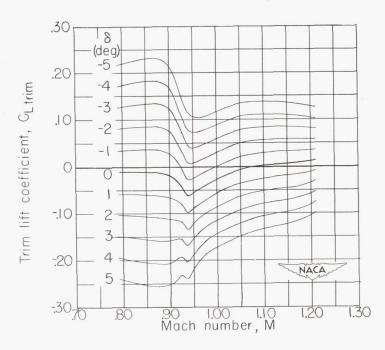
Figure 12.- Change in lift coefficient with respect to angle of attack as a function of Mach number.

(a) Center of gravity at 25 percent M.A.C.

(b) Center of gravity at 20 percent M.A.C.

Figure 13.- Variation of trim lift coefficient with Mach number for various elevator deflections for two center-of-gravity locations.
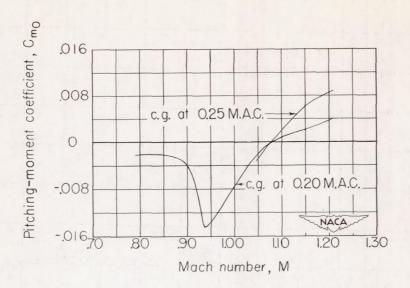
Figure 14.- Variation of the basic untrimmed pitching-moment coefficient
with Mach number.
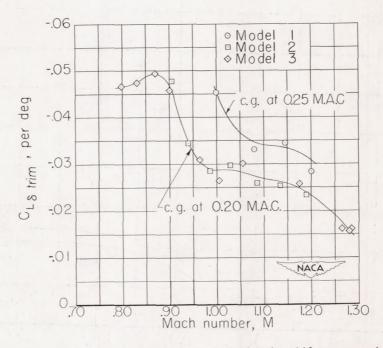
Figure 15.- Change in trim lift coefficient with respect to elevator
deflection as a function of Mach number.
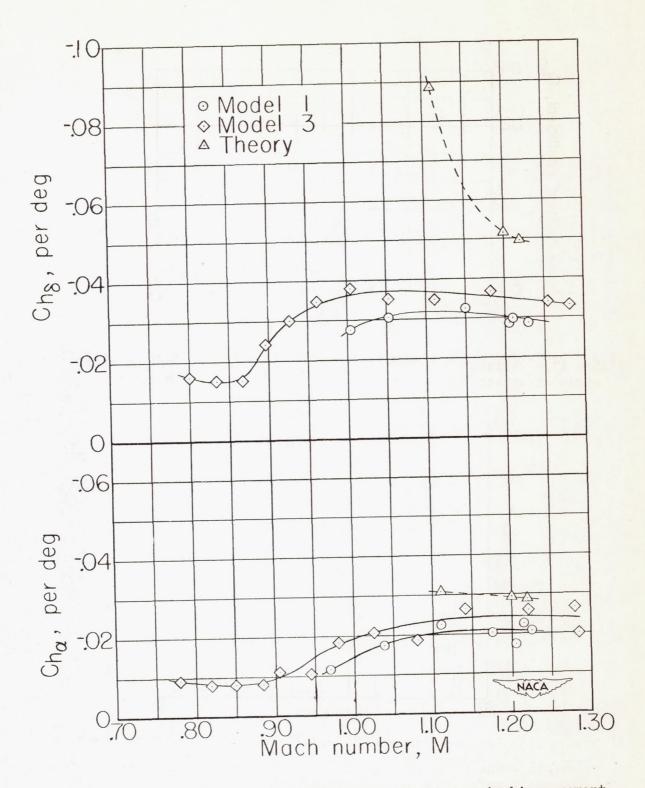
Figure 16.- Variation with Mach number of the change in hinge-moment
    coefficients with respect to angle of attack and elevator
    deflection.
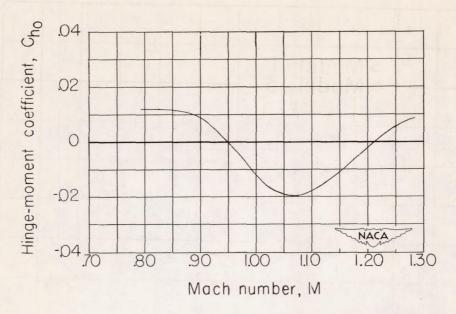
Figure 17.- Variation of the basic hinge-moment coefficient at zero
angle of attack and zero elevator deflection with Mach number.
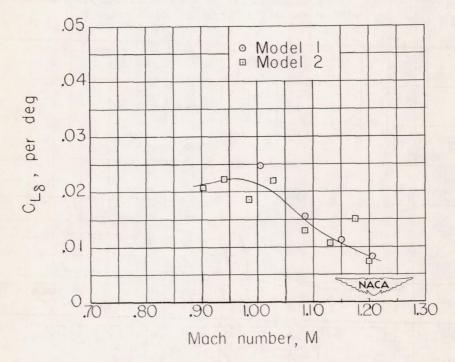
Figure 18.- Change in lift coefficient with respect to elevator
deflection as a function of Mach number.
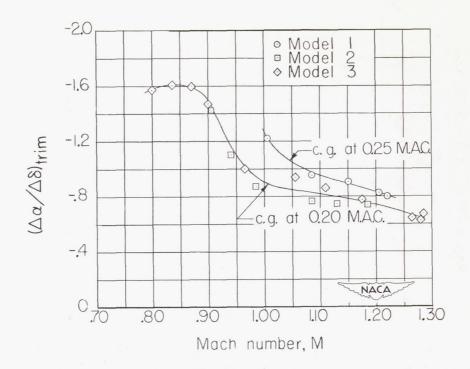
Figure 19.- Change in trim angle of attack with respect to elevator deflection as a function of Mach number.
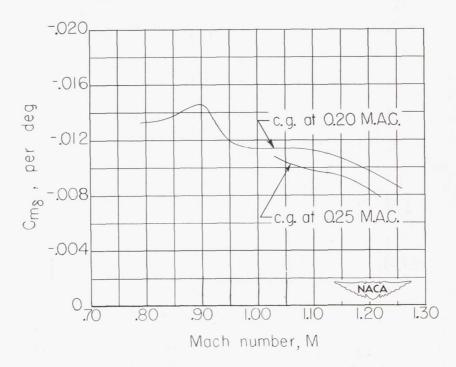
Figure 20.- Change in pitching-moment coefficient at a constant angle of attack with respect to elevator deflection as a function of Mach number.
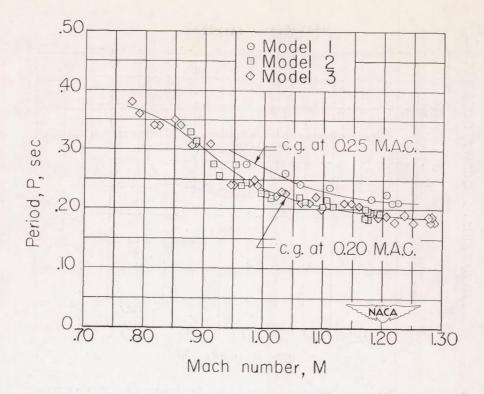
Figure 21.- Period of the short-period longitudinal oscillations as a function of Mach number.
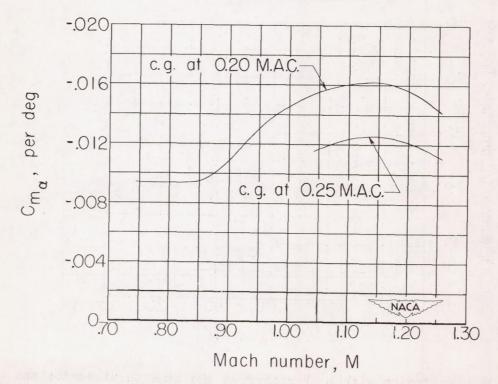
Figure 22.- Pitching-moment-coefficient slope with respect to angle of attack as a function of Mach number.
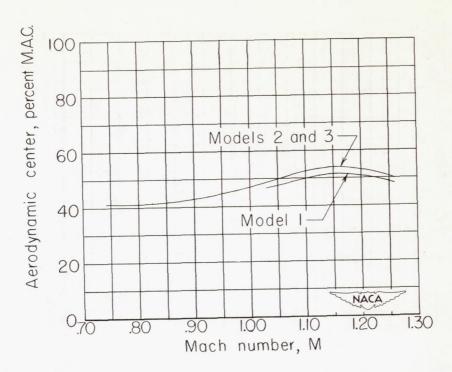
Figure 23.- Aerodynamic-center position in percent of the mean aerodynamic chord as a function of Mach number.
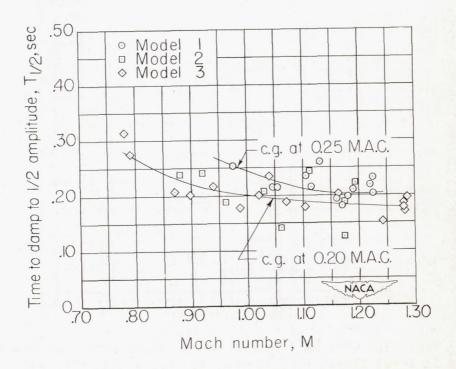
Figure 24.- Variation with Mach number of the time required for the short-period longitudinal oscillations to damp to one-half amplitude.
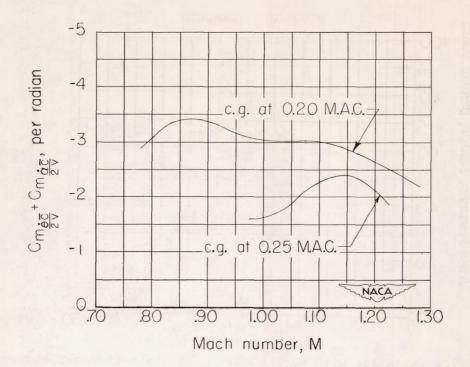
Figure 25.- Variation of the total damping coefficient with Mach number.
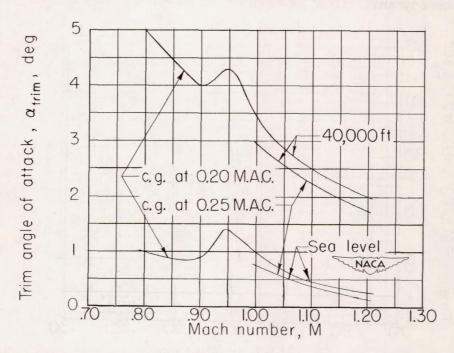
Figure 26.- Variation with Mach number of the angle of attack required for trim in level flight at different altitudes and center-of-gravity locations.
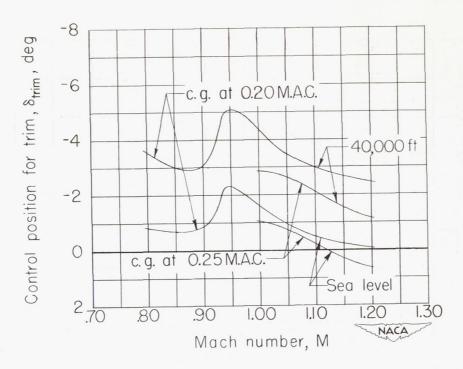
Figure 27.- Variation with Mach number of the elevator deflection required for trim in level flight at different altitudes and center-of-gravity locations.
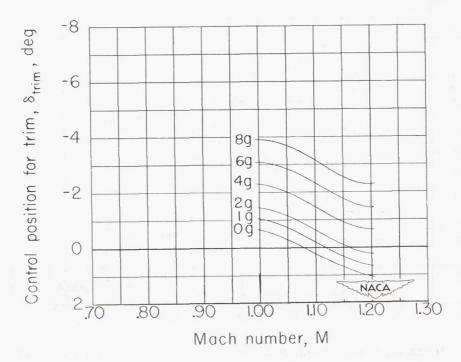
Figure 28.- Variation with Mach number of the elevator deflection required to produce various normal accelerations at sea level with the center of gravity at 25 percent mean aerodynamic chord.
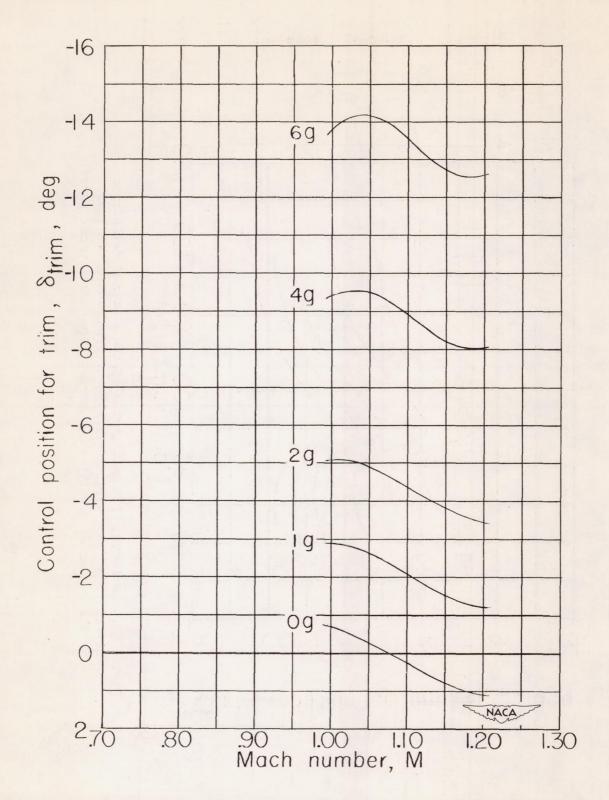
Figure 29.- Variation with Mach number of the elevator deflection required to produce various normal accelerations at 40,000 feet with the center of gravity at 25 percent mean aerodynamic chord.
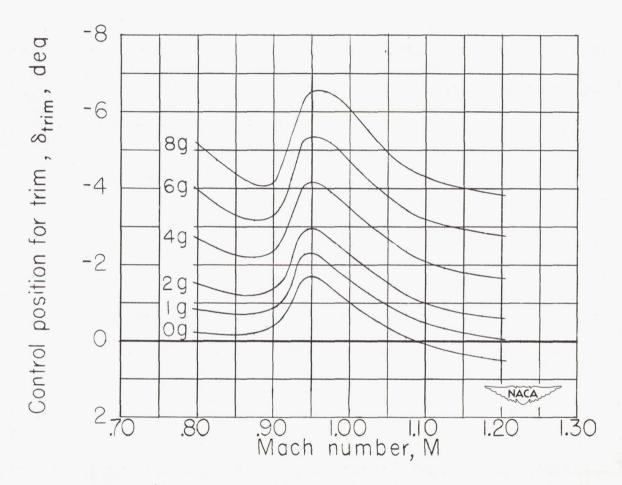
Figure 30.- Variation with Mach number of the elevator deflection required to produce various normal accelerations at sea level with the center of gravity at 20 percent mean aerodynamic chord.
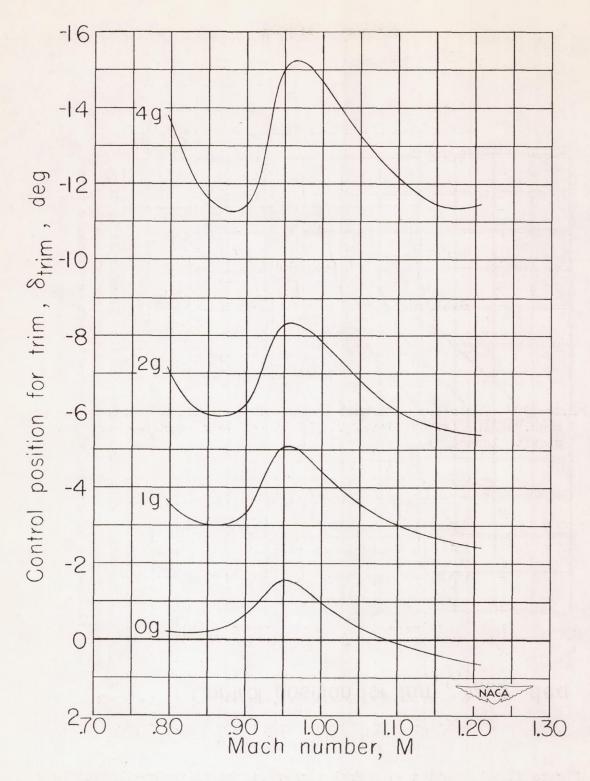
Figure 31.- Variation with Mach number of the elevator deflection required to produce various normal accelerations at 40,000 feet with the center of gravity at 20 percent mean aerodynamic chord.
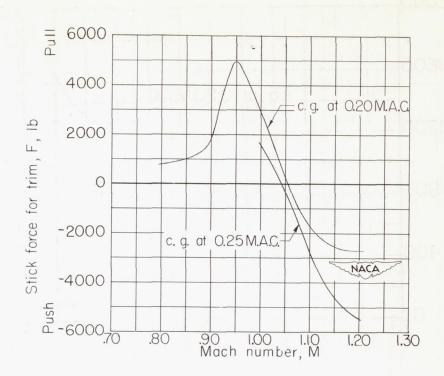
Figure 32.- Variation with Mach number of the elevator-control force
required for trim in level flight at sea level for two center-of-
gravity locations.
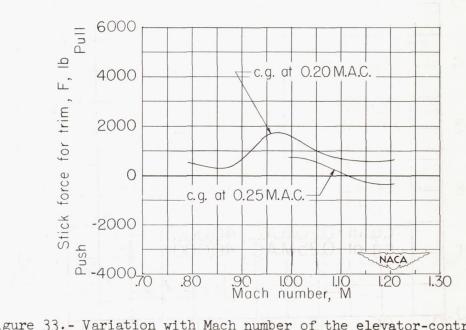
Figure 33.- Variation with Mach number of the elevator-control force
required for trim in level flight at 40,000 feet for two center-
of-gravity locations.
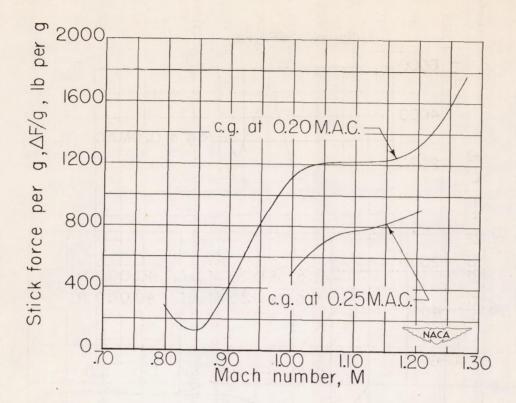
Figure 34.- Variation of the stick force per g with Mach number for different center-of-gravity locations.
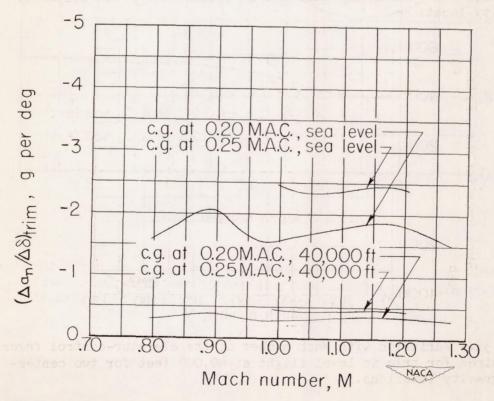
Figure 35.- Variation with Mach number of the normal acceleration produced per unit elevator deflection at different altitudes and center-of-gravity locations.
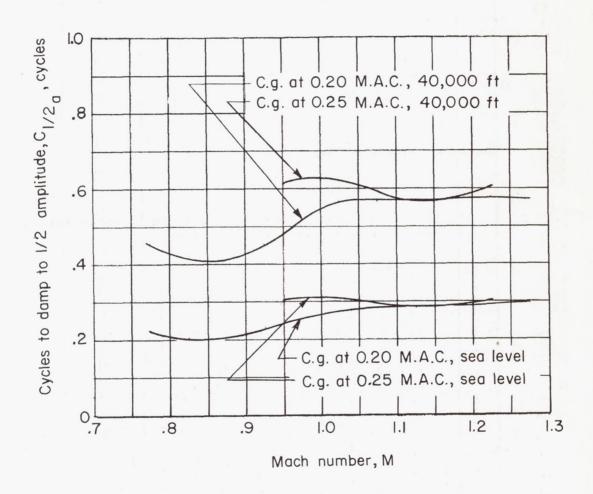
Figure 36.- Variation with Mach number of the cycles required for the
short-period longitudinal oscillations of the full-scale configu-
ration to damp to one-half amplitude at different altitudes and
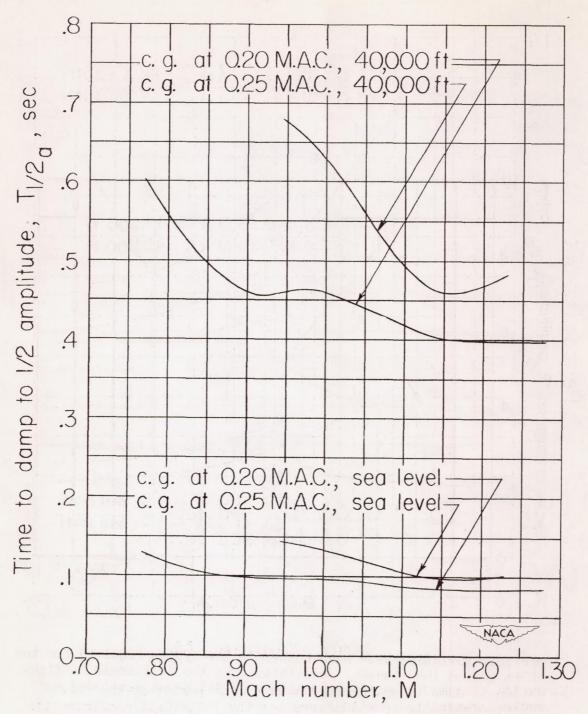center-of-gravity locations.

Figure 37.- Variation with Mach number of the time required for the
short-period longitudinal oscillations of the full-scale configu-
ration to damp to one-half amplitude at different altitudes and
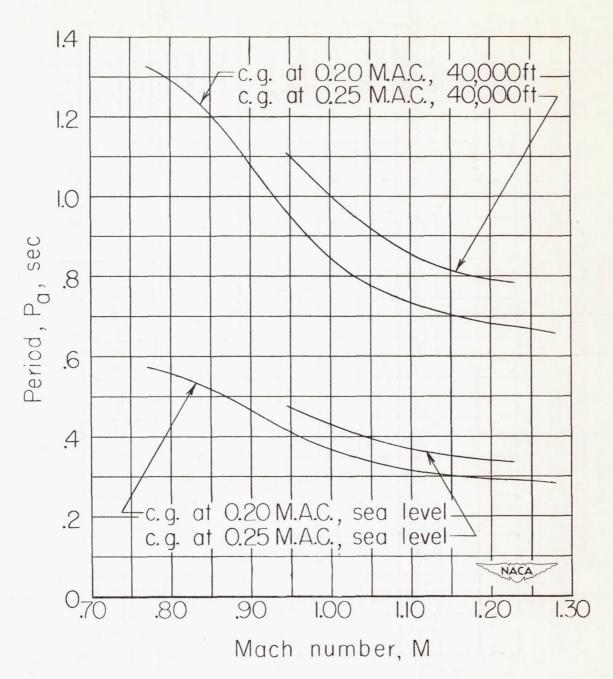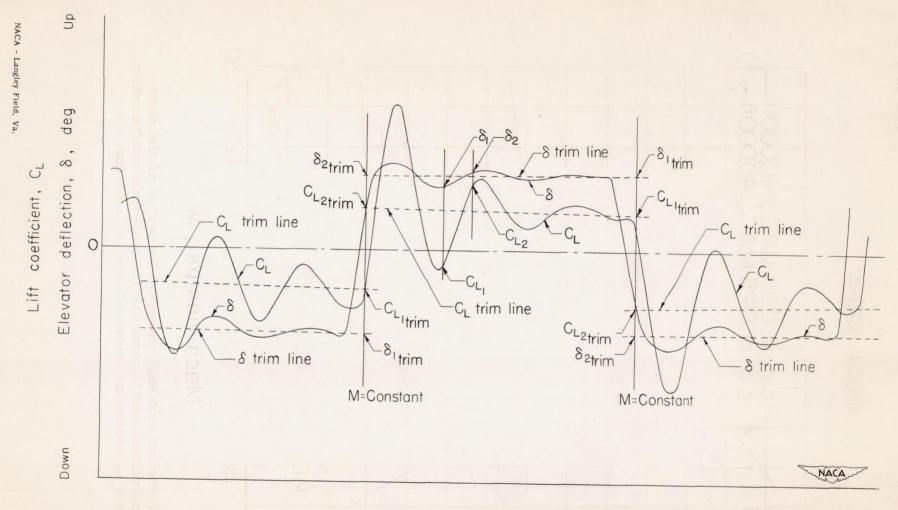center-of-gravity locations.

Figure 38.- Variation with Mach number of the period of the short-period longitudinal oscillations for the full-scale configuration at different altitudes and center-of-gravity locations.

Figure 39.- Typical section of time history as used for data analysis.

Time from launching, t, sec